SAND2011-4275C

Shock Tube Investigation of Unsteady Drag in Shock-Particle Interactions

Justin L. Wagner,[1] Steven J. Beresh,[2] Sean P. Kearney,[3] Brian O. Pruett,[4] and Elton Wright[5]
Sandia National Laboratories, Albuquerque, NM, 87185

A reassessment of historical drag coefficient data for spherical particles accelerated in shock-induced flows has motivated new shock tube experiments of particle response to the passage of a normal shock wave. Particle drag coefficients were measured by tracking the trajectories of 1-mm spheres in the wake of incident shocks of Mach numbers 1.68, 1.93, and 2.05. Data clearly show that as the Mach number increases, the drag coefficient increases substantially, consistent with past experiments. This increase significantly exceeds the drag predicted by incompressible standard drag models, but recently developed compressible drag models return values quite close to the current measurements. Low values for the acceleration parameter indicate that unsteadiness should not be expected to contribute to the drag increase. These observations suggest that elevated particle drag coefficients can be attributed to increased compressibility rather than flow unsteadiness.

A_c = acceleration parameter
C_D = sphere drag coefficient
M = Mach number
P = static pressure
Re = Reynolds number
a = speed of sound
d = sphere diameter
t = time
T = static temperature
u = streamwise velocity
x = streamwise coordinate
ρ = density
μ = dynamic viscosity

Subscripts
0 = arrival time of incident shock at sphere
1 = initial driven gas
2 = downstream of the initial shock
4 = initial driver gas
p = particle (sphere)
s = shock

[1] Senior Member of the Technical Staff, Engineering Sciences Center, P.O. Box 5800, Mailstop 0825; jwagner@sandia.gov. AIAA Member.
[2] Principal Member of the Technical Staff, Engineering Sciences Center, AIAA Associate Fellow.
[3] Principal Member of the Technical Staff, Engineering Sciences Center, AIAA Associate Fellow.
[4] Senior Technologist, Engineering Sciences Center.
[5] Senior Technologist, Engineering Sciences Center.

This work is supported by Sandia National Laboratories and the United States Department of Energy. Sandia is a multiprogram laboratory operated by Sandia Corporation, a Lockheed Martin Company, for the United States Department of Energy's National Nuclear Security Administration under Contract DE-AC04-94AL85000.

I. Introduction

Shock-particle interactions are fundamental in a multitude of engineering problems, but uncertainties in the unsteady particle response behind the shock wave hinder the ability to model and predict such flows. The most fundamental parameter that must be understood is the particle drag coefficient C_D. A variety of researchers over several decades have measured and correlated C_D in wind tunnels, ballistics ranges, and shock tubes; some of these experiments are reviewed by Igra and Ben-Dor [1] and Igra and Takayama [2]. In most practical situations, the dependence of the drag coefficient reduces to only two parameters, the particle Reynolds number based on the velocity difference:

$$Re_p = \rho_2 |u_2 - u_p| d_p / \mu_2 \tag{1}$$

and the particle Mach number based on the velocity difference:

$$M_p = |u_2 - u_p| / a_2 \tag{2}$$

where ρ_2, u_2, μ_2, and a_2 are the density, velocity, viscosity, and speed of sound in the gas behind the shock wave, respectively; u_p is the particle velocity; and d_p is the particle diameter.

A correlation describing C_D as a function of Re_p and M_p (or only Re_p for incompressible cases) has become known as the "standard drag curve" when it applies to steady flows, although several such "standards" exist. The most famous probably is that compiled in Hoerner [3], which also is found in numerous fluid dynamics textbooks. Henderson's correlation [4] is widely cited as well. Another useful example is the piecewise curve fit for incompressible conditions by Clift, Grace, and Weber [5] (reproduced in Ref. [1]), which covers an enormous range of Reynolds numbers; because it can be cumbersome to use, the single equation of Clift and Gauvin [6] (reproduced in Ref. [7]) is a close replacement for reasonable Reynolds numbers. Loth [7] modified this latter equation to account for compressibility, and Parmar et al [8] took a different approach to add compressibility through a new piecewise curve. The point at which compressibility becomes significant varies somewhat between authors, but is often agreed upon to lie somewhere between $M_p \approx 0.3$ and $M_p \approx 0.6$.

Though some differences exist in the predicted values of C_D returned by these various standard drag curves, they all are intended for use in a steady flow. When applied to unsteady flows, apparent discrepancies arise. A number of studies have measured higher values of C_D for an unsteady flow than would be predicted by a standard drag model [2, 9-12]. In such cases, unsteadiness refers to the acceleration of a particle at rest when subjected to the flow behind a shock wave, or the deceleration of a particle in a ballistic test. These unsteady effects continue to occur long after passage of the shock wave over the particle, which produces an additional effect. A transient spike in drag is known to occur as the shock passes over a sphere, but lasts only for microseconds for particle sizes typical in shock tube and ballistics tests [13-15]. In most experiments, therefore, this transient drag rise is immeasurable and does not contribute to the particle motion when measurements commence subsequent to the immediate shock passage.

Unfortunately, in many experiments, it has proven difficult to separate unsteady effects from other influences upon the drag; for example, some early experiments that showed elevated C_D concluded that the cause was not due to unsteadiness, but rather, likely due to particle roughness or asymmetry or some other indeterminate effect [16-18]. Scatter in the data of individual experiments also clouds the results. Nonetheless, Igra and Takayama [2] were able to conclude that the particle C_D in their shock tube experiment significantly exceeded standard drag predictions over a wide range of Reynolds numbers. From their data, they produced a new correlation to represent unsteady values of C_D. Jourdan et al [12] later revisited these experiments and produced a new data set with some improvements in the experimental methodology. Although they generated a different correlation for C_D, they arrived at the same conclusion that C_D remained elevated over an equivalent unsteady value. Suzuki et al [11] support these findings using a particle-injection method that significantly reduced the scatter of their data compared to previous efforts..

The point at which unsteady effects become significant can be defined by the acceleration parameter A_c:

$$A_c = \frac{du_p}{dt} d_p / \left(u_2 - u_p\right)^2 \tag{3}$$

using the same terms as previously [2, 16, 17]. Unsteady effects are considered negligible if $A_c \ll 1$ (Refs. [2, 16]), which in practice corresponds to roughly $A_c < 0.1$ according to Igra and Takayama [2] or $A_c < 0.01$ according to Crowe et al [16]. The liquid phase study of Karanfilian and Kotas [19] suggests that the drag coefficient increase for $A_c = 0.01$ would be about 1% and for $A_c = 0.1$ would be about 10%. Therefore, if A_c is small for an experiment, a standard drag model would be expected to predict the results – or, conversely, an elevated value of C_D would be attributable to some explanation other than unsteadiness.

With this consideration in mind, the shock tube studies of Igra and Takayama [2], Suzuki et al [11], and Jourdan et al [12] were re-examined. All the data for which the flow conditions could be determined are shown in Fig. 1, along with the standard drag prediction of Clift and Gauvin [6]. Despite the considerable degree of scatter in the data, it is evident that the values of C_D generally lie above the standard drag curve. However, this is not necessarily a result of the particle acceleration behind the shock wave in comparison to the steady flow inherent in the standard drag curve. Igra and Takayama demonstrate that for all of their data, $A_c < 0.1$; Jourdan et al state that $A_c < 0.035$; and an estimate of Suzuki et al's experiment yields $A_c < 0.01$ for all cases. Therefore, the effects of unsteadiness on C_D are expected to be small, suggesting that the elevated values of C_D detected in these experiments have some other source.

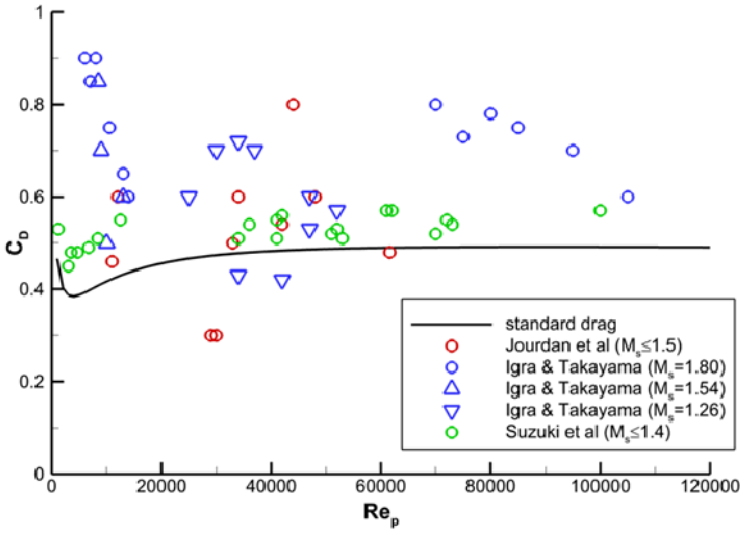

Fig. 1 Particle drag coefficients reproduced from Refs. [2, 11, 12] compared to the standard drag prediction of Ref. [6].

A possible explanation lies in the compressibility of the flow. At the time the cited experiments were conducted, the only known standard drag prediction to include compressibility was that of Henderson [4], which predicted a minimal effect (about 3%) for even the largest M_p in the data reproduced in Fig. 1. Based on this, the authors of the studies comprising Fig. 1 felt justified in neglecting the compressibility of their flow despite M_p as high as 0.85. Recently, both Loth [7] and Parmar et al [8] have produced new standard drag models that predict significantly higher effects due to compressibility. To examine whether compressibility may explain the elevated C_D in Fig. 1, the data were replotted in Fig. 2 as the difference between the measured values of C_D and two different standard drag models, one incompressible and one compressible. As can be seen, many of the data points shift closer to zero when compared with Loth's compressible model rather than Clift and Gauvin's incompressible model, indicating less discrepancy between the measured data and the prediction. The data points for relatively low shock Mach numbers M_s typically show minimal alteration when the compressible model is used, but the data for the largest Mach number display a considerably reduced discrepancy. This suggests that inclusion of compressibility into the standard drag model can more accurately predict the drag coefficient, and can explain the elevated C_D values seen in Fig. 1 without consideration of unsteady effects, consistent with the low values of A_c. Similar results were obtained comparing with Parmar et al's model rather than Loth's. The deviation in Igra and Takayama's data below Re_p of 10000 probably has a different explanation, as these used particularly lightweight foam particles.

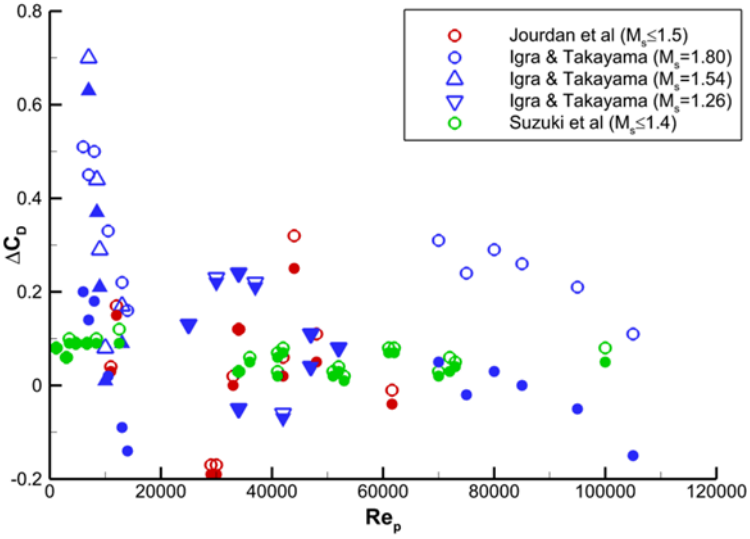

Fig. 2: Difference in measured particle drag coefficients [2, 11, 12] from the standard drag model of Clift and Gauvin [6] (hollow symbols) and the compressible drag model of Loth [7] (filled symbols).

Although reassessing past data with recent compressible drag predictions suggests that compressibility explains the drag increase, this is difficult to state conclusively given the significant scatter in the data and some uncertainty

in the flow conditions and particle characteristics. New experiments are necessary to establish that the elevated values of C_D can be explained by compressibility rather than unsteadiness, which has motivated the present shock tube study.

II. Experimental Setup

A. Multiphase Shock Tube

A schematic of the multiphase shock tube used to test the acceleration of spheres in shock-induced flows is shown in Fig. 3, which is a modification of a facility used for previous studies of shock interaction with dense particle fields [20, 21]. The driver section is a 2.1 m long stainless steel pipe with an inner diameter of 88.9 mm and a wall thickness of 12.7 mm. A high-pressure compressed nitrogen system provides the driver gas. The pressurization of the driver pipe and surge tanks is controlled remotely with an in-house developed LabVIEW (National Instruments) code that instructs a Tescom (Model 26-2065-B24A352) dome-loaded pressure regulator system and various solenoid valves. The driver gas pressure P_4 and the surge tank pressure are monitored with an Omega pressure transducer (Model PX01C1-1KG5T). A port on the driver end plate provides access for a thermocouple (T-type) to monitor the driver gas temperature T_4, which is typically near 296 K. Cruciform scored, nickel alloy burst disks (BS&B Safety Systems) are used as the diaphragms that initially separate the driver gas from the driven gas. The scoring of the burst disk ensures it opens in four petals preventing fragmentation. As seen in Fig. 3, the burst disk holder section follows the driver pipe. This section is circular with an inner diameter that matches the driver pipe and it has a length of 157.5 mm. Burst disks with nominal burst pressures of 1100 kPa (160 psig) and 2760 kPa (400 psig), and 4140 kPa (600 psig) are used to produce nominal shock Mach numbers of 1.68, 1.93, and 2.05. According to the manufacturer, burst pressures are repeatable to 5%, which corresponds to a shot-to-shot burst uncertainty time of about 5 seconds [20].

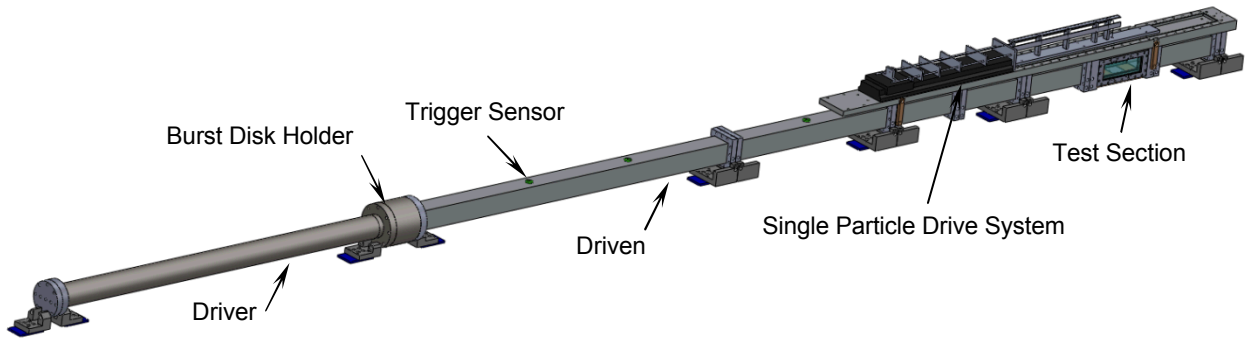

Fig. 3 Schematic of the multiphase shock-tube with the single-particle apparatus.

The driven section consists of seven pieces made from extruded square aluminum tubing having a nominal wall thickness of 12.7 mm. The total driven length is 5.2 m. The first two driven sections have a nominal inner width of 76.2 mm. The inner walls of the last five sections have a width of 79.2 ± 0.2 mm. A driven section with parallel planar walls was chosen to simplify the design and configuration of instrumentation such as pressure transducers and optical diagnostics systems. The modular design of the driven section allows for the simple insertion of a test section. Typically, the driven gas is ambient air at an initial temperature of about 300 K and an initial atmospheric pressure of about 83 kPa. An Omega pressure transducer (Model PX01C1-1KG5T) and a thermocouple (T-type) are used to measure the driven initial conditions. Measurements [20] show that the shock develops a very nearly planar front upon reaching the test section location. The arrival of the reflected shock at the test section limits the useful test times to about 2 – 3 ms. Additional details on the shock tube design and operations are provided in [20].

Experimental test conditions are presented in Table 1. Flush-mounted PCB pressure sensors (Model 113B27) are placed 203 mm upstream 69 mm downstream of the test section centerline (pressure measurement details are given below). The crossing times from these sensors are used to calculate the incident shock velocity W_s and Mach number M_s. The experimental parameters presented in Table 1 are based on five tests each.

Table 1: Shock Tube Experimental Conditions

M_s	P_4, kPa	P_1, kPa	T_4, K	T_1, K	W_s, m/s
1.66 ± 0.03	1242 ± 45	83.4 ± 0.2	298 ± 2	296.0 ± 0.5	579 ± 7
1.93 ± 0.02	2935 ± 170	83.5 ± 0.4	299 ± 2	296.4 ± 0.8	666 ± 8
2.05 ± 0.01	4170 ± 350	83.2 ± 0.2	297 ± 1	296.3 ± 1.5	707 ± 3

B. Single-Particle Drive System and Test Section

A schematic of the system used to insert spheres into the shock tube test section is shown in Fig. 4. Prior to a test, about 500 individual 1 mm stainless steel spheres having a density of 7612 kg/m^3 are loaded into a sphere holder tube having a diameter of 1.1 mm. Since the uncertainty in the time of diaphragm burst is about 5 seconds, many spheres can be dropped to ensure that one will be present in the test section upon arrival of the incident shock. The spheres are manufactured by CCR Products, and according to the manufacturer have diameter and sphericity tolerances of 0.0003, and 0.0002 mm, respectively. The drive system attaches to a mounting plate that is bolted to the top of the shock tube. The angle of the top of the mounting plate is 0.5-degrees with respect to the horizontal to prevent the spheres from rolling into the test section prematurely. A precision Aerotech linear motor (Pro165LM) drives a 0.90 mm push rod into the sphere holder tube. To prevent buckling of the thin push rod, rod guides are also driven by the motor along two shafts. The motor is controlled with a PC and an in-house developed LabVIEW (National Instruments) code. The spheres fall out of the tube through a 1.1 mm hole in the test section ceiling. The spheres that fall through the test section prior to arrival of the incident shock travel exit through a 6 mm hole in the floor into a 6 mm collector tube. The number of spheres present in the test section can be controlled by varying the speed of the motor. To obtain the drag of single spheres the motor is typically run at speeds of 25-75 mm/s. Since the shock and post-shock velocities are much higher than those of the particle prior to shock, the particle is essentially 'frozen' with respect to the incident shock and its downward motion is negligible.

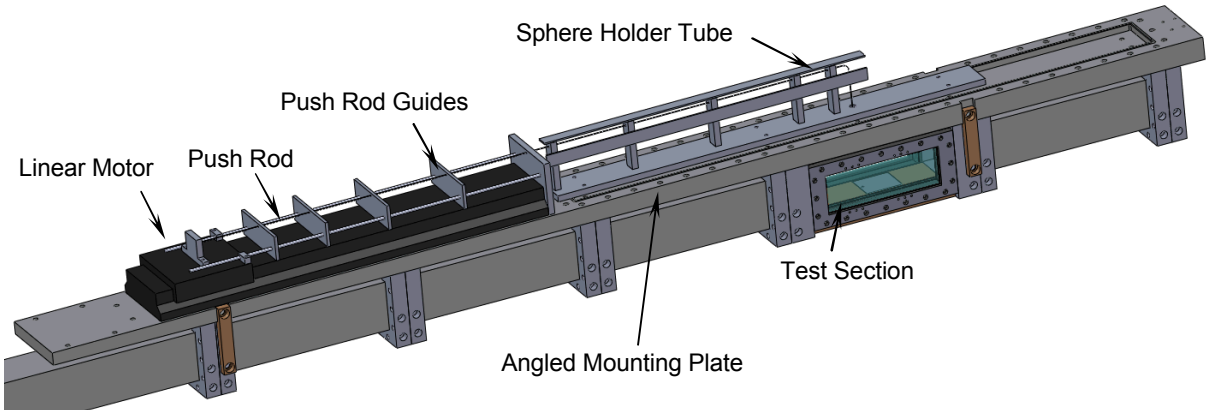

Fig. 4 Schematic of showing a closer view of the single-particle drive system and test section.

C. Fast-Response Pressure Measurements

In addition to the sensors used to measure M_s, additional flush-mounted PCB pressure sensors (Model 113B27, or Model 113B26) are placed throughout the shock tube. As shown in Fig. 3, a sensor about 0.5 m downstream of the diaphragm is used to trigger the data acquisition systems. In this paper $x = 0$ corresponds to the initial sphere location at $t = 0$, which is the arrival time of the incident shock. Four sensors are placed near $x = 0$ to characterize the incident shock and its induced flow during a test. One sensor is mounted in the ceiling at about $x = 64$ mm and three sensors are placed at $x = 10$, 41, and 64 mm along the shock tube floor.

Additional pressure measurement hardware includes a signal conditioner box (PCB Model 483C) that provides the transducers the constant current and the excitation voltage necessary for operation. The signal conditioner also amplifies the sensor signals. The amplified signals are then low-pass filtered (Krohn-Hite Model 3384) with a cutoff frequency of 1 MHz. The filtered signals are sent to a data acquisition chassis (NI PXI 1505), in which two 14-bit

data acquisition cards (NI PXI 6133) digitize the signals at a sampling frequency of 2.5 MHz. The digitized signals are then sent through fiber optic cables to a personal computer where they are recorded.

D. High-Speed Schlieren Imaging System

A high-speed schlieren imaging system was used to study the particle motions that occur following the arrival of the incident shock. The light source was a Visual Instrumentation Corporation continuous-wave high brightness LED (Model 900415). To collimate the source, a 50.8 mm diameter biconvex lens with a focal length of 0.5 m was used. To focus on the knife-edge, a 50.8 mm diameter plano-convex lens with a focal length of about 0.8 m was used. The images were acquired with a Phantom digital camera (v12.1) having a resolution at full-frame of 1280 × 800 pixels. Two fields of view were used with the first having dimensions of about 50 × 25 mm^2 and the second 50 × 50 mm^2 The larger field of view was chosen in instances to increase the likelihood for a particle in the field of view upon arrival of the incident shock and the smaller field of view was chosen to have an increased framing rate. For the smaller field-of-view the framing rate was 100 kHz, and the image resolution was 304 × 128 pixels. For the larger field-of-view the framing rate was 51 kHz, and the image resolution was 304 × 256 pixels. The exposure time for both fields-of-view was 1 μs. Each image was saved in 8-bit format.

III. Data Analysis

A. Particle Tracking Velocimetry (PTV)

The sphere drag coefficients are based on velocities obtained from particle tracking velocimetry data, which were generated using high-speed schlieren images. An example of such a sequence of schlieren images acquired

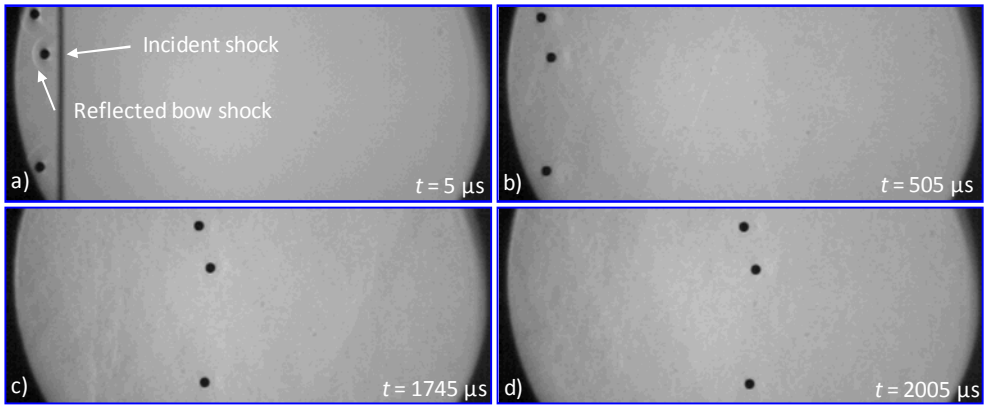

Fig. 5 Sample schlieren images for a Mach 1.68 test with three particles within the field-of-view at times: a) t = 5 μs, b) t = 505 μs, c) t = 1745 μs, and d) t = 2005 μs.

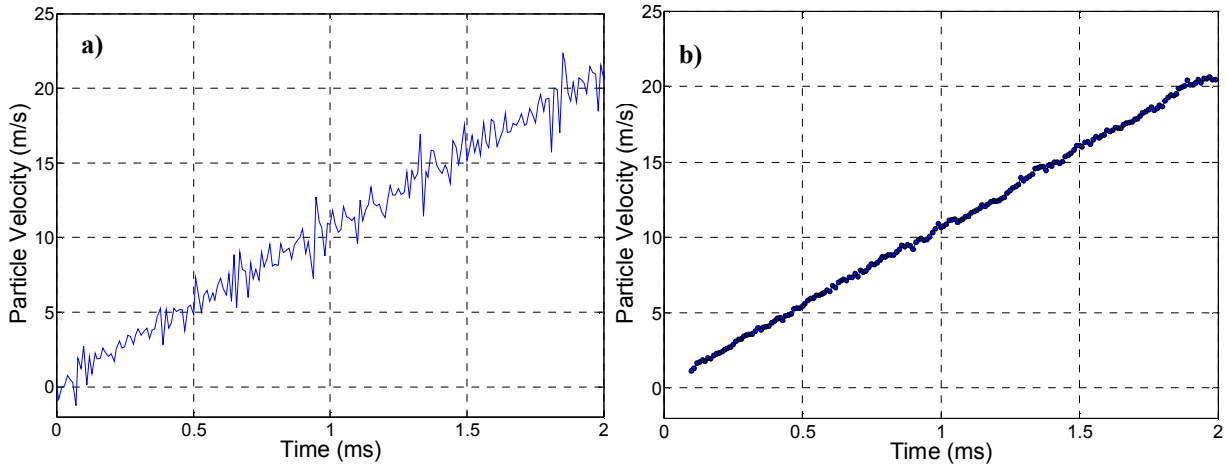

Fig. 6 PTV: a) Raw PTV data, and b) 9-point (90 μs) smoothed PTV data.

during a Mach 1.68 test at a framing rate of 100 kHz is shown in Fig. 5. Three particles appear in the sequence. As will be discussed, particle-particle interactions in this particular test were not significant enough to cause a measurable difference in drag coefficient between the three spheres. In each schlieren image, the particles appear in shadow with a diameter of about 6 pixels. In Fig.5a, at t = 5 μs, the incident shock has passed over the particles. Reflected bow shocks appear, which are a transient effect of the since the induced at this time the particle Mach number is about 0.75. With continuing time the bow shocks propagate upstream until they are no longer present in the field of view. From t = 5 – 2005 μs, the three particles propagate downstream through the field of view.

Using the particle shadows during propagation, the particle velocity was computed using the PTV algorithm implemented in the software package in Davis 7.4. Prior to PTV processing, each raw image was inverted using a threshold of about 80 counts. The inverted images were then processed with PTV using validation filters to limit the maximum particle velocities and accelerations to reasonable values. The PTV data for the lower-most sphere of Fig. 5 are given in Fig. 6. Raw PTV data are shown in Fig. 6a and the data smoothed with a nine-point centralized (90 μs) moving average filter are given in Fig. 6b. From Fig. 6a, the apparent noise in the PTV data is about 1-3 m/s, which corresponds to about 0.1-0.2 pixels of particle displacement. For about the first 0.1-0.2 ms of particle travel, the displacements were small enough (less than about 0.1-0.2 pixels,) to therefore be within the noise and to render the PTV data unreliable. Thus, these data points are not included in the drag coefficient calculations. The PTV data for the higher two nominal shock Mach numbers exhibited similar characteristics to that in Fig. 6, except with higher velocity magnitudes and accelerations.

B. Drag Coefficient Determination

The sphere drag coefficient was determined by fitting the particle velocities to the drag relation. The drag relation for an accelerating sphere in a constant velocity fluid is [2]:

$$C_D = \frac{4\rho_p d_p \frac{\partial u_p}{\partial t}}{3\rho_2 (u_2 - u_p)^2} \tag{4}$$

Solving the drag equation for u_p yields:

$$u_p = u_2 - \frac{u_2}{u_2 A t + 1} \tag{5}$$

where

$$A = \frac{3\rho_2 C_D}{4\rho_p D_p} \tag{6}$$

Then by least squares regression, Eq. (5) is fit to the velocity data to determine the one unknown parameter, C_D. As indicated by Eq. (5) and Eq. (6), an accurate measurement of C_D requires knowledge of the fluid properties around the immersed sphere. In the case of the present data, it is assumed that the flow properties remain constant during the times where C_D is computed. Pressure traces in the vicinity of the sphere were used to assess the validity of this assumption. An example trace is shown in Fig. 7. Following the pressure increase caused by the incident shock, the pressure is relatively constant. While it is difficult to discern small changes in flow velocity and density from such a pressure trace, the relatively constant pressure indicates that large flow variances do not occur over the 2 ms test time.

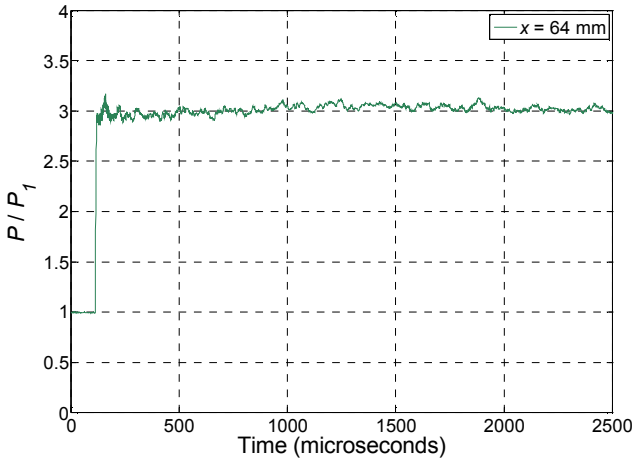

Fig. 7 Ceiling pressure during the M_s = 1.68 test of Fig. 3 and Fig.4.

In Fig. 8, least squares fits of the particle velocity predicted by Eq. (5) are compared to the PTV data of Fig. 6b. Over the 2 ms data acquisition time Re_p decreases from about 25,000 to 23,000, while M_p changes from about 0.75 to 0.7. The correlation of Parmar et al. [8] suggests that C_D should decrease by about 6% over this 2 ms. To evaluate if such a change could be detected in the data, a piecewise fit of Eq. (5) was applied where the segment length was 0.5 ms. The method gave drag coefficients of 0.55, 0.54, 0.54, and 0.55 for the times of 0-0.5, 0.5-1.0, 1.0-1.5, and 1.5-2 ms, respectively. The piecewise fit is shown in Fig. 8. The fact that C_D varies so little without a clear trend over the data acquisition period suggests that the piecewise method for measuring C_D is

unable to resolve any small changes that may be occurring over the rather limited range of flow conditions range tested. In comparison, a constant C_D = 0.55 fit to the data is also shown in Fig. 8. Since a discernable difference was not obtained using the piecewise method, the constant C_D method is used herein.

The top two particles seen in Fig. 5 were also measured to have C_D = 0.55. This suggests that the in-plane spacing (note that the spanwise spacing is not known) of the top two particles was great enough to preclude particle-particle interactions that could cause a significant change in drag. Although, as is discussed below, this was not found to be the case for measurements made for the two higher shock Mach numbers.

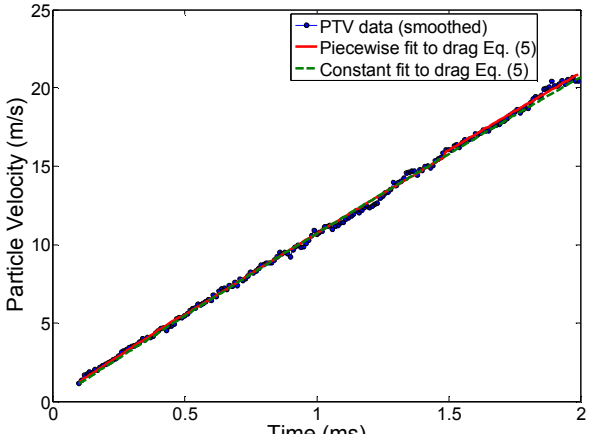

Fig. 8 PTV data and fits based on drag relation Eq (5).

IV. Discussion of Results

A sequence of images acquired during a M_s = 2.05 test is depicted in Fig. 9. The initial particle Mach number is about 1. In comparison to the lower Mach number test of Fig. 5 where M_2 = 0.75, the effects of compressibility are naturally much more pronounced and recompression shocks are observed in the particle's wake. The extent of the recompression shocks is seen to increase in the images from t = 19 through 58 µs. A greater particle Mach number also significantly increases the drag coefficient. For example, using the method described above, C_D was measured to be 0.83, or about 50% greater than the case of Fig. 5.

Increasing the particle Mach number from about 0.75 through 1 was also observed to significantly increase the distance for which particles interact. This result is not surprising when considering the nearly normal waves that occur in a near sonic flow around a sphere. Examples of such interactions are shown in the sequence of Fig. 10.

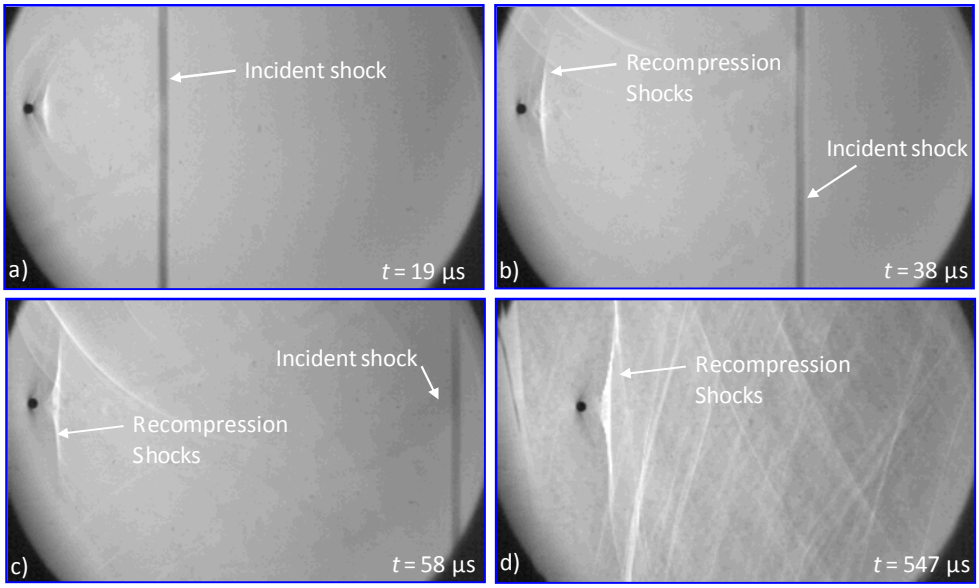

Fig. 9 Schlieren images for a Mach 2.05 test at times: a) t = 19 µs, b) t = 38 µs, c) t = 58 µs, and d) t = 547 µs.

Similar to the single sphere sequence in Fig. 9, as the time increases from 6 through 45 µs, the recompression shocks grow in size. Eventually they interact as is evident in Fig. 10d. The drag coefficient for the bottom most sphere in Fig. 10 calculated to be 0.94, which will be shown to be well outside of the scatter for measurements of single spheres in similar flows. Again, the spanwise separation of the spheres was not measured so it is difficult to currently determine exactly how the sphere separation modifies the drag. What can be concluded is that it is

necessary to omit data for which particle-particle interactions occur, or the drag coefficients may be found artificially high with a greater degree of scatter.

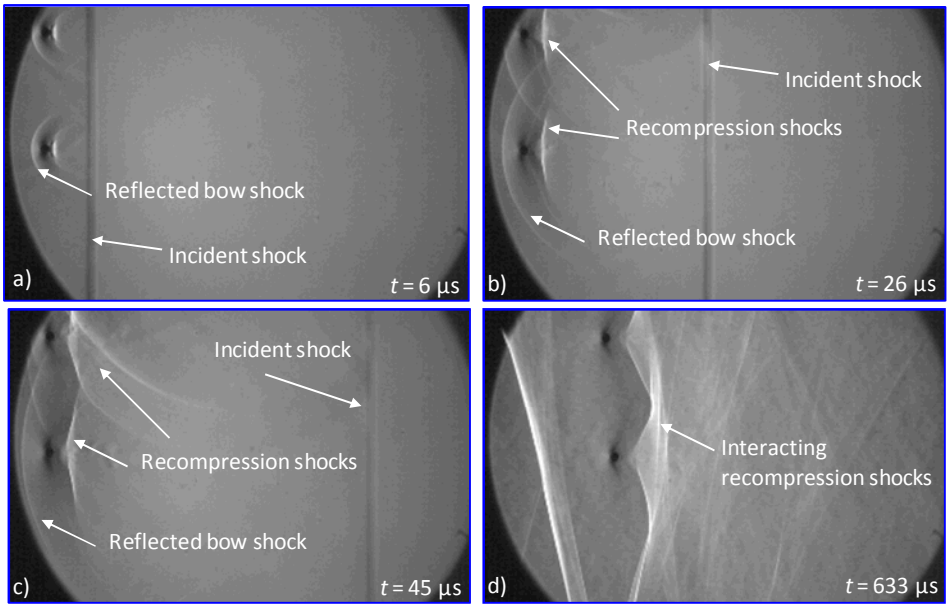

Fig. 10 Schlieren images showing two interacting spheres during a Mach 2.02 test at times: a) t = 6 µs, b) t = 26 µs, c) t = 45 µs, and d) t = 547 µs.

Table 2: Shock Tube Experimental Conditions for a 1mm sphere having a density of 7612 kg/m^3

Run #	M_s	M_2	T_2, K	ρ_2, kg/m^3	U_2, m/s	Δt (ms)	M_p (range)	Re_p (range)	A_c	C_D
121a	1.68	0.75	428	2.12	312	0.1-2.0	0.75-0.70	27000-25300	0.0001	0.55
121b	1.68	0.75	428	2.12	312	0.1-2.0	0.75-0.70	27000-25300	0.0001	0.55
121c	1.68	0.75	428	2.12	312	0.1-2.0	0.75-0.70	27000-25300	0.0001	0.55
128	1.67	0.74	425	2.11	307	0.1-2.0	0.74-0.70	26600-25000	0.0001	0.52
129	1.68	0.76	428	2.14	314	0.1-2.0	0.75-0.70	27400-25600	0.0001	0.55
135	1.94	0.92	485	2.52	408	0.1-1.2	0.92-0.85	38400-35400	0.0002	0.73
136	1.93	0.92	485	2.52	407	0.1-1.2	0.92-0.85	38400-35500	0.0002	0.71
145a	1.92	0.91	481	2.50	402	0.2-1.2	0.90-0.84	37300-34600	0.0002	0.76
145b	1.92	0.91	481	2.52	402	0.2-1.2	0.90-0.84	37400-34700	0.0002	0.75
150	1.93	0.91	487	2.52	404	0.2-1.2	0.90-0.84	37400-34700	0.0002	0.72
167	2.05	0.99	511	2.68	447	0.1-0.8	0.99-0.91	43300-40000	0.0002	0.83
172	2.05	0.99	511	2.69	449	0.1-0.7	0.99-0.92	43600-40600	0.0002	0.82
174	2.05	0.99	512	2.67	448	0.1-0.8	0.99-0.91	43200-39800	0.0002	0.83
175	2.04	0.99	512	2.67	447	0.1-1.0	0.99-0.88	43100-38700	0.0002	0.84

With the above considerations in mind, extra care was taken at the two higher Mach numbers to only include sphere trajectories for which particle-particle interactions were not present. The results at all three nominal test conditions are summarized in Table 2. For each test, the conditions in the shock-induced flow computed from normal shock theory are given. Also noted is the time for which the particle was tracked Δt to determine its drag and the corresponding particle Mach and Reynolds number ranges during this time. The acceleration parameter, computed from the measured C_D and Eqs. (3) and (4) is also given. In all cases $Ac < 0.0003$. Therefore, flow unsteadiness is not expected to play a noticeable role in increasing the particle drag [2, 16]. On the other hand, it is evident from Table 2 that as flow compressibility increases with M_p, so does C_D. In summary for the three nominal M_2 values of 0.75, 0.92, and 0.99, the mean C_D computes to 0.54 ± 0.03, 0.74 ± 0.06, and 0.83 ± 0.05. The uncertainty bands correspond to 95% confidence intervals based on student-t theory.

The data suggest that increased compressibility is the cause of the increased sphere drag and not flow unsteadiness. It is also useful to compare the current measurements to correlations that include Mach number such as the classic relation of Henderson [4] and the two more recent forms given by Loth [7] and Parmar et al. [8]. Figure 11 shows such a comparison to the current M_p = 0.99 data. The data lie substantially above the Henderson [4] curve, which highlights how previous researchers such as Suzuki et al. [11] may have reached the conclusion that compressibility could not have explained their observed drag increase. However, a comparison of the current data to that of more recent correlations is highly suggestive that compressibility is fact the cause.

The current data for all three Mach numbers are plotted with the correlations of Loth [7] and Parmar et al. [8] in Fig. 12. The measurements at a nominal M_2 of 0.75 agree quite well with the Parmar et al. correlation, while as M_2 increases, the current drag coefficients tend to fall closer to those predicted by Loth. Although it is not clear which correleation performs better, it is evident that compressibility, or Mach number of the induced flow, correlates well with the increased drag

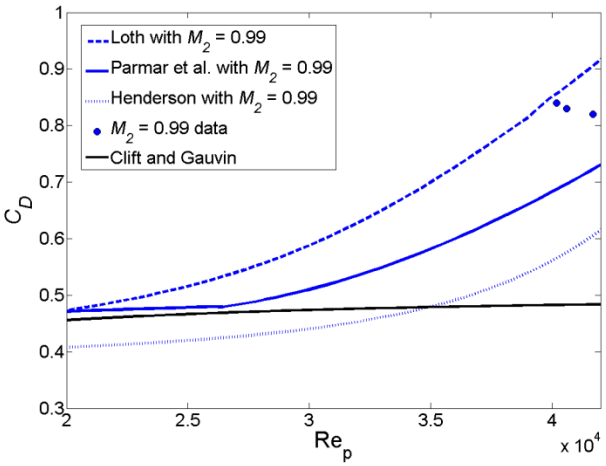

Fig. 11 Comparison of M_s = 2.05 (M_2 = 0.99) data to correlations of Loth [7], Parmar et al. [8], Henderson [4], and Clift and Gauvin [6]. The correlation curves were generated using the average initial conditions found in Table 1.

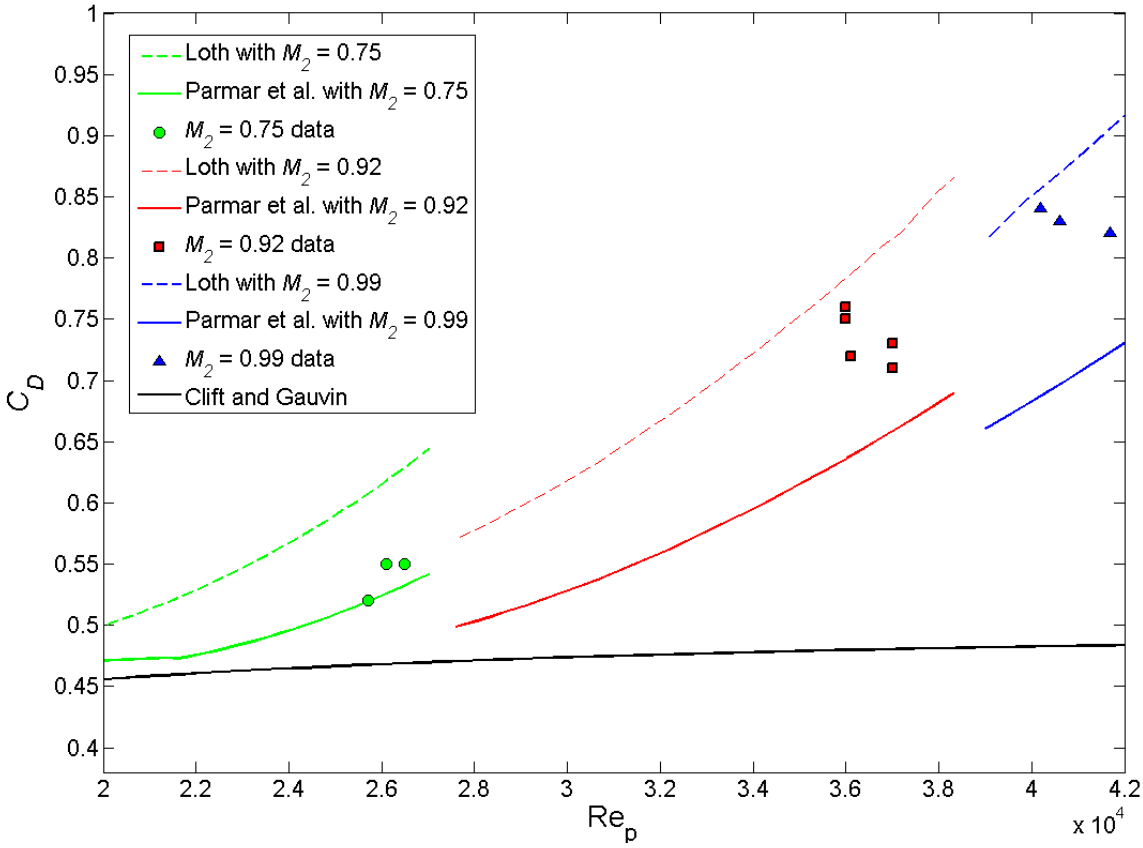

Fig. 12 Comparison of current data to correlations of Loth [7], Parmar et al. [8], and Clift and Gauvin [6]. The correlation curves were generated using the average M_2, computed from the average M_s and initial conditions found in Table 1.

coefficients. The current results are therefore supportive of the argument that the increased drag coefficients of spheres having low acceleration parameters reported in previous shock tube studies [2, 9-12] can be attributed to compressibility rather than flow unsteadiness. Other factors may play a role as well in some experiments, such as freestream turbulence levels or particle roughness or asymmetry.

V. Conclusions

New drag coefficient data for spheres accelerated in shock-induced flows have been obtained. The motivation for the experiments was to determine if compressibility and as opposed to flow unsteadiness was the cause of the increased drag frequently reported to occur for shock-accelerated particles.

The velocities of 1 mm stainless steel spheres were measured during shock tube tests using particle tracking velocimetry at shock Mach numbers of 1.68, 1.93 and 2.05. The particle drag coefficients were then determined by fitting the velocity measurements to the drag relation. Data acquired over an induced flow Mach number range of about 0.7 to 1.0 clearly show that increasing the particle Mach number increases its drag coefficient. Values of C_D are found to increase from 0.54 ± 0.03 at a particle Mach number of 0.7 to 0.83 ± 0.05 at a Mach 1.0. Furthermore low values for the acceleration parameter indicate that flow unsteadiness is not expected to account for an increased sphere drag for this new data. Therefore it is concluded that the increased drag coefficients measured in the current work are caused by increased compressibility and not flow unsteadiness, which additionally suggests a similar explanation for many previous shock tube experiments.

Acknowledgments

This work was supported by an internal Laboratory Directed Research and Development (LDRD) grant. The authors gratefully acknowledge this source of support. The authors thank Wayne Trott, Jaime Castaneda and Melvin Baer for their suggestions during the early design phases of the experiment.

References

[1]Igra, O., and Ben-Dor, G., "Dusty Shock Waves," *Applied Mechanics Reviews*, Vol. 41, No. 11, 1988, pp. 379-437.

[2]Igra, O., and Takayama, K., "Shock Tube Study of the Drag Coefficient of a Sphere in a Non-stationary Flow," *Proceedings of the Royal Society of London A*, Vol. 442, 1993, pp. 231-247.

[3]Hoerner, S. F., *Fluid-Dynamic Drag*, published by the author, Brick Town, NJ, 1965.

[4]Henderson, C. B., "Drag Coefficients of Spheres in Continuum and Rarefied Flows," *AIAA Journal*, Vol. 14, No. 6, 1976, pp. 707-708.

[5]Clift, R., Grace, J. R., and Weber, M. E., *Bubbles, Drops, and Particles*, Academic, New York, NY, 1978.

[6]Clift, R., and Gauvin, W. H., *Proceedings of CHEMECA '70*, Vol. 1, Butterworth, Melbourne, 1970, pp. 14-28.

[7]Loth, E., "Compressibility and Rarefaction Effects on Drag of a Spherical Particle," *AIAA Journal*, Vol. 46, No. 9, 2008, pp. 2219-2228.

[8]Parmar, M., Haselbacher, A., and Balachandar, S., "Improved Drag Correlation for Spheres and Application to Shock-Tube Experiments," *AIAA Journal*, Vol. 48, No. 6, 2010, pp. 1273-1276.

[9]Rodriguez, G., Grandeboeuf, P., Khelifi, M., and Haas, J. F., "Drag Coefficient Measurement of Spheres in a Vertical Shock Tube and Numerical Simulation," *Proceedings of the 19th International Symposium on Shock Waves*, Marseille, France, July 1993, pp. 43-48.

[10]Devals, C., Jourdan, G., Estivalezes, J. L., Meshkov, E. E., and Houas, L., "Shock Tube Spherical Particle Accelerating Study for Drag Coefficient Determination," *Shock Waves*, Vol. 12, 2003, pp. 325-331.

[11]Suzuki, T., Sakamura, Y., Igra, O., Adachi, T., Kobayashi, S., Kotani, A., and Funawatashi, Y., "Shock Tube Study of Particles' Motion Behind a Planar Shock Wave," *Measurement Science and Technology*, Vol. 16, 2005, pp. 2431-2436.

[12]Jourdan, G., Houas, L., Igra, O., Estivalezes, J. L., Devals, C., and Meshkov, E. E., "Drag Coefficient of a Sphere in a Non-Stationary Flow," *Proceedings of the Royal Society A*, Vol. 463, 2007, pp. 3323-3345.

[13]Tanno, H., Itoh, K., Saito, T., Abe, A., and Takayama, K., "Interaction of a Shock with a Sphere Suspended in a Vertical Shock Tube," *Shock Waves*, Vol. 13, No. 3, 2003, pp. 191-200.

[14]Sun, M., Saito, T., Takayama, K., and Tanno, H., "Unsteady Drag on a Sphere by Shock Wave Loading," Shock Waves, Vol. 14, No. 1-2, 2004, pp. 3-9.

[15]Skews, B. W., Bredin, M. S., and Efune, M., "Drag Measurement in Unsteady Compressible Flow; Part 2: Shock Wave Loading of Spheres and Cones," *R&D Journal of the South African Institute of Mechanical Engineering*, Vol. 23, No. 1, 2007, pp. 13-19.

[16]Crowe, C. T., Nicholls, J. A., and Morrison, R. B., "Drag Coefficients of Inert and Burning Particles Accelerating in Gas Streams," *Symposium (International) on Combustion*, Vol. 9, No. 1, 1963, pp. 395-406.

[17]Selberg, B. P., and Nicholls, J. A., "Drag Coefficient of Small Spherical Particles," *AIAA Journal*, Vol. 6, No. 3, 1968, pp. 401-408.

[18]Rudinger, G., "Effective Drag Coefficient for Gas-Particle Flow in Shock Tubes," *ASME Journal of Basic Engineering*, Vol. 92, 1970, pp. 165-172.

[19]Karanfilian, S. K., and Kotas, T. J., "Drag on a Sphere in Unsteady Motion in a Liquid at Rest," *Journal of Fluid Mechanics*, Vol. 87, Part 1, 1978, pp. 85-96.

[20]Wagner, J. L., Beresh, S. J., Kearney, S. P., Trott, W. M., Castaneda, J. N., Pruett, B., Cooper, M. A., Baer, M. R., "Development of a Multiphase Shock Tube for Energetic Materials Characterization," AIAA Paper 2010-4535, June 2010.

[21]Wagner, J. L., Beresh, S. J., Kearney, S. P., Trott, W. M., Castaneda, J. N., Pruett, M. A., Baer, M. R., "Interaction of a Planar Shock with a Dense Field of Particles in a Multiphase Shock Tube," AIAA Paper 2011-188, January 2011.